RSC Advances

PAPER

View Article Online
View Journal | View Issue

Cite this: *RSC Adv.*, 2016, **6**, 89708

Single layer PbI_2: hydrogenation-driven reconstructions†

C. Bacaksiz*[a] and H. Sahin[b]

By performing density functional theory-based calculations, we investigate how a hydrogen atom interacts with the surfaces of monolayer PbI_2 and how one- and two-side hydrogenation modifies its structural, electronic, and magnetic properties. Firstly, it was shown that the T-phase of single layer PbI_2 is energetically more favorable than the H-phase. It is found that hydrogenation of its surfaces is possible through the adsorption of hydrogen on the iodine sites. While H atoms do not form a particular bonding-type at low concentration, by increasing the number of hydrogenated I-sites well-ordered hydrogen patterns are formed on the PbI_2 matrix. In addition, we found that for one-side hydrogenation, the structure forms a (2 × 1) Jahn–Teller type distorted structure and the bandgap is dramatically reduced compared to hydrogen-free single layer PbI_2. Moreover, in the case of full hydrogenation, the structure also possesses another (2 × 2) reconstruction with a reduction in the bandgap. The easily tunable electronic and structural properties of single layer PbI_2 controlled by hydrogenation reveal its potential uses in nanoscale semiconducting device applications.

Received 9th June 2016
Accepted 1st September 2016

DOI: 10.1039/c6ra15020a

www.rsc.org/advances

I. Introduction

After a decade of research which was triggered by the synthesis of graphene,[1] the theoretical prediction and synthesis of many 2D ultrathin materials such as silicene,[2,3] germanene,[2,4,5] stanene,[6,7] transition metal dichalcogenides (TMDs),[8–15] hexagonal III–V binary compounds (h-BN, h-AlN)[16–19] and metal hydroxides ($Ca(OH)_2$, $Mg(OH)_2$)[20,21] have been achieved. However, recent research efforts have been directed towards not only the synthesis of graphene-like materials, but also towards the functionalization of existing ultra-thin crystal structures. These recent studies have revealed some important results such as (i) tunable bandgap opening in graphene,[22–27] (ii) H-defect-induced magnetization of graphane,[27,28] (iii) bandgap engineering in silicene and germanene,[29–31] (iv) stability enhancement in h-BN,[32] and (v) tunable magnetic features in TMDs.[33,34]

One of the most recently synthesized single layer semiconductors is lead iodide (PbI_2). In bulk PbI_2, which is a member of the metal halide family, van der Waals-stacked individual layers form an octahedral T-phase. As a precursor material for lead iodide perovskites, given by the general formula CH_3NH_3-$PbI_{3-n}X_n$ (X = Cl, Br), PbI_2 has been used in many different device applications.[35–39] Recently, by performing optical measurements and first-principles calculations of bulk and few-layer PbI_2, Toulouse *et al.* showed that the exciton binding energy dramatically increases with a decreasing number of layers.[40] In addition, the synthesis of monolayer PbI_2 within carbon nanotubes was reported by Cabana *et al.*[41] In recent work, Zhou *et al.* investigated the structure, stability, electronic and optical properties of monolayer PbI_2 and also the hetero-bilayer form with graphene by using first principles calculations.[42] However, to our knowledge, the interaction between a hydrogen (H) atom and the surface of monolayer PbI_2 and how the physical properties are affected under hydrogenation are still open questions.

In this study, using first principles calculations based on density functional theory (DFT), we investigate the interaction of hydrogen atoms with bare single layer PbI_2. We also focus on the structural and electronic properties of half- and fully-hydrogenated monolayers of PbI_2. We found that the T-phase is energetically more favourable than the H-phase and it is an indirect semiconductor. Our investigation revealed that chemical functionalization by both half and full hydrogenation cause reconstruction in the structure of monolayer PbI_2 and lead to a significant reduction in the bandgap of the structure. Such a hydrogen-driven reconstruction in monolayers of PbI_2 has not been reported before.

The paper is organized as follows: in Section II we give details of our computational methodology. An overview of the structural phases and the electronic properties of monolayer hexagonal PbI_2 are presented in Section III. In Section IV we focus on the interaction between a single hydrogen atom and monolayer PbI_2. The effects of one-side hydrogen coverage, in other words half-hydrogenation, of monolayer PbI_2 are given in Section V, and after that the properties of fully-hydrogenated monolayer PbI_2 are presented in Section VI. Finally, we present our conclusion in Section VII.

[a]Department of Physics, Izmir Institute of Technology, 35430 Izmir, Turkey
[b]Department of Photonics, Izmir Institute of Technology, 35430 Izmir, Turkey

† PACS numbers: 71.15.Mb, 73.20.Hb, 73.22.-f, 73.61.−r, 73.90.+f.

II. Computational methodology

We perform the structural optimization and molecular dynamics (MD) simulations by using the Vienna *ab initio* simulation package, VASP[43–45] which is based on density functional theory (DFT). To describe electron exchange and correlation, the Perdew–Burke–Ernzerhof (PBE) form of the generalized gradient approximation (GGA)[46] was adopted. The vdW forces, which are effective in the intralayer interaction, were taken into account by using the DFT-D2 method of Grimme.[47,48] To obtain the charge distribution of the configuration, Bader charge analysis was used.[49,50] The stability of the resulting structures was examined with *ab initio* MD calculations.

The following parameters were used for the analyses. The total energy difference between the sequential steps in the iterations was taken to be 10^{-5} eV for the convergence criterion. The convergence for the Hellmann–Feynman forces on each unit cell was taken to be 10^{-4} eV Å^{-1}. A 0.05 eV Gaussian smearing factor was used and the pressures on the unit cell were decreased to a value of less than 1.0 kB in all three directions. For the determination of accurate charge densities, Brillouin zone integration was performed using a 12 × 12 × 1 Γ-centered mesh for the primitive unit cell. To avoid interactions between adjacent PbI_2 configurations, our calculations were performed with a large unit cell including a 16 Å vacuum space.

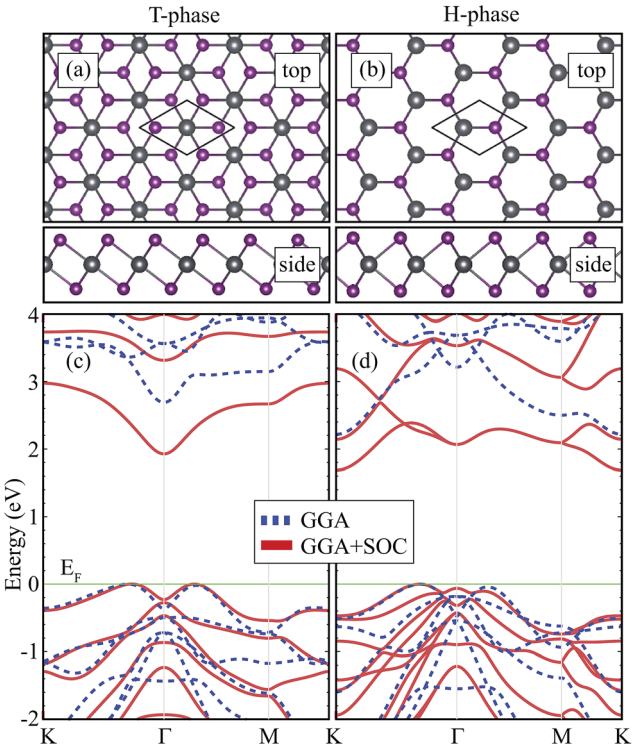

Fig. 1 (a) and (b) illustrate the structure of monolayer 1T and 1H PbI_2, respectively. (c) and (d) are the corresponding band structures where the blue and red curves represent GGA and GGA + SOC, respectively. The Fermi level (E_F) is given by the green solid line.

III. H and T phases of single layer PbI_2

Similarly to TMDs, monolayer PbI_2 can form two different phases, octahedrally coordinated 1T and trigonal-prismatic coordinated 1H. As shown in Fig. 1, both phases have three trigonal subplanes where the Pb subplane is sandwiched by two I-subplanes. While the 1T phase is a member of the $P\bar{3}m2$ space group where subplanes of it are *ABC* stacked, the 1H phase is a member of the $P\bar{6}m2$ space group where subplanes of it are *ABA* stacked. The lattice vectors of both phases are $\mathbf{v}_1 = a\left(\frac{1}{2}, \frac{\sqrt{3}}{2}, 0\right)$, $\mathbf{v}_2 = a\left(\frac{1}{2}, -\frac{\sqrt{3}}{2}, 0\right)$ where $|\mathbf{v}_1| = |\mathbf{v}_2|$ and a is the lattice constant. The atomic coordinates of the 1T phase are $\left(\frac{|v_1|}{2}, \frac{|v_1|}{2}, 0\right)$, $\left(\frac{|v_1|}{6}, \frac{|v_1|}{6}, \frac{c}{2}\right)$, and $\left(\frac{5|v_1|}{6}, \frac{5|v_1|}{6}, -\frac{c}{2}\right)$ for the Pb and two I atoms, respectively, where c is the distance between the subplanes of I atoms. The atomic coordinates of the 1H phase are given as $\left(\frac{|v_1|}{3}, \frac{|v_1|}{3}, 0\right)$, $\left(\frac{2|v_1|}{3}, \frac{2|v_1|}{3}, \frac{c}{2}\right)$, and $\left(\frac{2|v_1|}{3}, \frac{2|v_1|}{3}, -\frac{c}{2}\right)$.

The lattice constants of the optimized crystal structures of the 1T and 1H phases are 4.44 Å and 4.32 Å, respectively. However, as shown in Table 1, the interatomic distance d_{Pb-I} of the T-phase (3.23 Å) is found to be shorter than that of the H-phase (3.26 Å). Total energy calculations also reveal that the 1T phase is 165 meV per unit cell more favourable than the H-phase. The cohesive energies per atom of the 1T and 1H phases are 2.76 and 2.70 eV, respectively. These results are consistent with the previous results which showed that the T-phase is the most favourable form of both bulk and monolayer crystals of PbI_2. In addition, the workfunctions (Φ) of the 1T and 1H phases are calculated to be 5.96 eV and 6.05 eV, respectively.

We also present the electronic energy band dispersions of the 1T and 1H phases (approximated by GGA and GGA + SOC) in Fig. 1(c) and (d), respectively. The 1T phase of the PbI_2 monolayer has an indirect bandgap where the valence band maximum (VBM) is between the K and the Γ symmetry points and the conduction band minimum (CBM) is at the Γ point. As given in Table 1, the energy bandgaps of the 1T phase are 2.69 and 1.93 eV within GGA and GGA + SOC. The total charge donated by each Pb atom is 0.9 and 0.8 e^- for the 1T and 1H phases, respectively. Moreover, the 1H phase also has an indirect bandgap where the VBM is between the K and the Γ points and CBM is at the K point. The bandgap of the 1H phase is calculated to be 2.22 eV within GGA and 1.68 eV within GGA + SOC, respectively.

It is seen that although the T and H phases have similar electronic characteristics at the valence band edges which are unmeasurable by experimental tools such as ARPES, the lattice parameter and the work function are unique features of each phase. Discussions in the following chapters will be performed on the 1T-phase that corresponds to the ground state crystalline structure of single layer PbI_2.

Table 1 Calculated parameters for monolayer PbI_2 are the lattice constant in the lateral direction, a; the atomic distance between Pb and I atoms, d_{Pb-I}; the charge transfer from the Pb to I atom, $\Delta\rho$; the work function, Φ; and the cohesive energy, E_c. E_g^{GGA} and $E_g^{GGA+SOC}$ are the energy bandgap values within GGA and GGA + SOC, respectively

	a (Å)	d_{Pb-I} (Å)	$\Delta\rho$ (e^-)	Φ (eV)	E_c (eV)	E_g^{GGA} (eV)	$E_g^{GGA+SOC}$ (eV)
1T PbI_2	4.44	3.23	0.9	5.96	2.76	2.69	1.93
1H PbI_2	4.32	3.26	0.8	6.05	2.70	2.22	1.68

IV. Interaction with a single hydrogen atom

For engineering the structural, electronic and magnetic properties of a material, surface hydrogenation is an easy and powerful method. From a theoretical point of view the determination of the interactions between the PbI_2 surface and H atoms is of importance.

For the calculation of the adsorption and diffusion characteristics of an H atom on the surface of monolayer PbI_2 a 3×3 supercell, which is large enough to avoid the interaction between adjacent H atoms, is used. First of all, to determine the most favourable adsorption site of the H atom, various initial positions over the surface are calculated: the top-Pb site, the midpoint of the Pb–I bond, the top-I site and the sites in between these points. As shown in Fig. 2(a), adsorption of a hydrogen atom in the vicinity of an I atom with a bond length of 1.66 Å is much more preferable than adsorption on the other lattice points. It is also seen that the formation of a tilted I–H bond with the surface leads to slightly out-of-plane relaxation of the underlying I atom. Considering its spin polarized ground state in a vacuum, the binding energy of a single H atom is calculated to be 0.32 eV which is quite small compared to the binding energy of H to graphene (0.98 eV).[51]

In addition, our Bader charge analysis reveals that the bonded H atom preserves its 1.0 e^-, on the other hand, the H bonded I atom has 7.0 e^- in contrast with the other I atoms which have 7.4 e^-. The displaced 0.4 e^- from that particular I atom is shared by the nearest three Pb atoms. Our analysis reveals that the H atom does not form a bond when the vdW term is excluded. Therefore, one can conclude that the bonding type of H with the PbI_2 surface is a weak vdW type bonding.

The single H bonded system has midgap states which originate from the H atom. When we consider these states, the bandgap is 0.21 eV as shown in Fig. 2(c). There is one localized band near the Fermi level which has a charge distribution as shown inset of Fig. 2(c). The system has a magnetic ground state with a magnetic moment of 1.0 μ_B. It also appears that only the states around the Fermi level have splitting due to hydrogen-induced magnetism.

To have a more general picture of the interaction between the H atom and the monolayer PbI_2, we perform the diffusion barrier calculation which is shown in Fig. 2(d). From the top of an I atom to top of its second nearest I atom, the energy difference plot shows that the top of the I atom possesses the minimum energy. The barrier to escape from the influence of the I atom is around 285 meV. There is one local minimum on the path which coincides with the center of the triangle of I atoms over the Pb atom. In addition, considering the energy plot around the I atom as a harmonic potential, the jump frequency of the H atom is estimated to be $\nu \approx 0.191$ GHz. These results are consistent with the MD simulations which reveal that at low temperatures (up to 50 K), single H rotates almost freely around the I atom. Although H is bonded to the underlying I, there is no certain preferable bonding direction with the PbI_2 surface.

V. One-side hydrogenation

Following the analysis of the interaction of H atom with the surface of PbI_2, in this section, we investigate how the structural, electronic and magnetic properties are modified upon the hydrogen coverage of the surfaces. Firstly, the half-hydrogenated (half-H-PbI_2) structure, with one-by-one hydrogen coverage of each I atom on the same surface, is investigated.

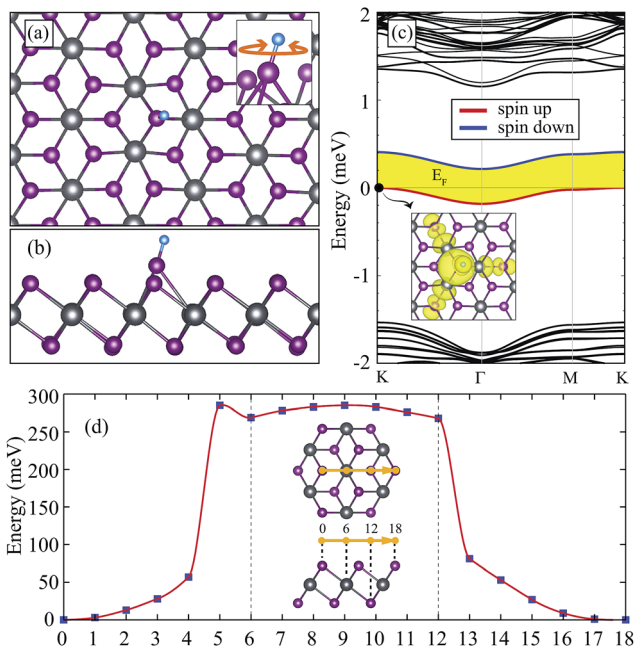

Fig. 2 (a) and (b) show the structure of H atom adsorbed (3×3) PbI_2 from the top and the side, respectively. The inset in (a) illustrates the rotation of H around the I atom. (c) is the band structure of the single H atom adsorbed 3×3 PbI_2 monolayer where the blue and red curves represent the different spin states. The inset shows the charge distribution of the VBM at Γ. The Fermi level (E_F) is given by the green solid line. (d) is the diffusion barrier plot through the given path.

As shown in Fig. 3(a) and (b), H atoms form a well-ordered crystal structure (where $\theta = 60°$) in the one-side covered structure. The lattice constant of this perfectly hexagonal crystal structure is calculated to be 4.05 Å. Compared to the hydrogen-free bare PbI_2 structure, the Pb–I bond length increases from 3.23 to 3.77 Å at the hydrogenated side. However, at the hydrogen-free side, Pb–I bonds become stronger and the bond length is calculated to be 3.08 Å. Moreover, alongside the structural changes, the half-hydrogenation also modifies the charge distribution in the crystal structure. Bader charge analysis shows that functionalization cancels the charge transfer between the Pb and I atoms at the hydrogenated side and therefore removes the ionic character of the Pb–I bond. In contrast, at the bare side of the half-H-PbI_2, the charge sharing increases where the I and Pb atoms have 7.4 and 3.5 e^-, respectively. Electronically, as shown in Fig. 3(f), the semiconducting character vanishes after hydrogenation and the system turns into a ferromagnetic metal with 0.14 μ_B per unit cell. However, hydrogenation-induced metalization in single layer PbI_2 requires further analysis.

For further analysis of the half-hydrogenated structure we also performed finite temperature MD calculations. Our calculations showed that starting from very low temperatures (20–25 K) half-H-PbI_2 tends to undergo a structural transformation. Apparently, the perfectly hexagonal half-hydrogenated structure mentioned before corresponds to a local minimum on the Born–Oppenheimer surface and for the determination of the ground state structure one needs a small perturbation such as temperature. Then, by performing full structural optimization of the distorted structure created by the MD calculation, we obtained the real ground state crystal structure of half-H-PbI_2.

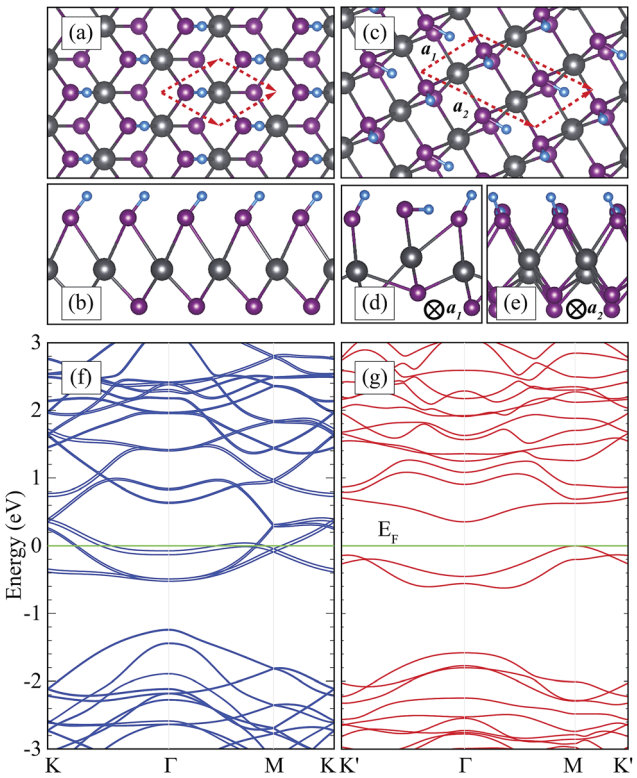

Fig. 3 The structures in (a) and (b) are for perfect hexagonal and (c), (d), and (e) are for distorted forms of half-hydrogenated monolayer PbI_2 (half-H-PbI_2). View directions are given in (d) and (e). (f) and (g) are the corresponding band structures. To compare the perfect and distorted forms, 2 × 2 unit cells are used for both band structures. The Fermi level (E_F) is given by the green solid line.

As shown in Fig. 3(c) and (d), the ground state of half-H-PbI_2 forms a (2 × 1) reconstructed surface. It is calculated that this (2 × 1) reconstructed phase of half-H-PbI_2 is 0.41 eV per unit cell more favourable than the perfectly hexagonal phase which is obtained by a total energy calculation performed at 0 K. In this half-H-PbI_2 structure, there are two bonding types of H atom. One H atom stands over the I atom at an angle of 28.5° to the normal of the structure plane, the other H reclines parallel to the surface at the level of the I atoms. The I–H bond lengths for the standing and reclined H atoms are 1.70 and 1.69 Å which are slightly larger than that of perfectly hexagonal phase (1.65 Å). The Pb–I bond length of the reconstructed phase is 3.93 Å at the hydrogenated side and the smallest Pb–I bond length is 3.11 Å at the hydrogen-free side. These values are larger than those of the perfectly hexagonal phase (3.77 and 3.08 Å, respectively). As given in Table 2, the lattice constants are 4.22 and 7.83 Å with an angle of 58.9° and the workfunction at the hydrogenated side is found to be 3.57 eV. On the other side, the H binding energy per H atom is 0.64 eV which is much larger than that of single H on the 3 × 3 supercell (E_{bind} = 0.32 eV for single H).

The charge distributions of the reconstructed structure are specific to the structurally different Pb, I, and H atoms. In general, with respect to the H atom bonding configurations, all of the atoms have a specific charge in the (2 × 1) reconstructed unit cell (see Fig. 3(c)–(e)). Briefly, the standing- and reclining-H atoms have 1.1 and 1.0 e^-; the I atoms bonded with standing- and reclining-H have 7.0 and 7.1 e^-; the Pb atoms close to standing- and reclining-H have 3.4 and 3.7 e^-, respectively. On the bare side of the half-H-PbI_2, the I atoms have larger charges of 7.3 and 7.4 e^- which are aligned in the *z*-axis with standing- and reclining-H, respectively.

Furthermore, upon the temperature-driven structural transformation from the perfectly hexagonal to the (2 × 1) reconstructed phase, not only the structure but also the electronic properties are modified dramatically. As shown in Fig. 3(g), the reconstruction removes the metallic properties and the system becomes a semiconductor with a small bandgap of 0.35 eV. The bandgap is still indirect in that the VBM and CBM are at the *M* and *Γ* points, respectively. After the reconstruction the system has a nonmagnetic ground state. This type of distortion is known as a Jahn–Teller distortion in which the dangling bonds are filled up and the system transforms from a metal to a semiconductor. Therefore, the semiconducting nature of the (2 × 1) reconstructed phase of half-H-PbI_2 that corresponds to the ground state structure is quite important for nanoscale optoelectronic device applications.

VI. Full hydrogenation

As well as the one-side hydrogenation that may be realized on a one-side-supported material, one can also achieve both-side

Table 2 Calculated parameters for half- and full-hydrogenated monolayer PbI_2 (half-H-PbI_2 and full-H-PbI_2) are the lattice constant in the lateral directions, $\mathbf{a}_1$ and $\mathbf{a}_2$; the angle between the lattice vectors, θ; the work function, Φ; the cohesive energy, E_c; the binding energy per H atom, E_{bind}; the bandgap, E_g^{GGA}; and the magnetic moment per primitive cell, μ

	$\mathbf{a}_1$ (Å)	$\mathbf{a}_2$ (Å)	θ (°)	Φ (eV)	E_c (eV)	E_{bind} (eV)	E_g^{GGA} (eV)	μ (μ_B)
Half-H-PbI_2	4.22	7.83	58.9	3.57	2.23	0.64	0.35	0.0
Full-H-PbI_2	8.29	8.02	63.0	3.73	2.03	0.93	0.76	0.0

coverage of monolayer PbI_2 (full-H-PbI_2) when it is in a free-standing form. Structural analysis of the full-H-PbI_2 is performed by applying the same methodology. MD calculations revealed that the ground state atomic structure of the full-H-PbI_2 is quite different from that of half-H-PbI_2.

Similarly to the half-hydrogenated structure, H-induced reconstructions take place starting from 20 to 25 K and therefore three different types of I–H bonds (perpendicular, a tilted bond at 44.8°, and the reclined bond parallel to the surface) are formed over the PbI_2 surface (see Fig. 4(a)–(c)). Then the analysis of the fully-optimized crystal structure reveals that the primitive unit cell of full-H-PbI_2 contains a (2 × 2) reconstructed phase of PbI_2H_2. In the reconstructed structure, the shortest Pb–I bond length is calculated to be 3.60 Å. The I–H bond length is around 1.68 Å which is very close to that of the single H adsorbed case. As given in Table 2, the lattice parameters of the (2 × 2) reconstructed structure are calculated to be 8.29 and 8.02 Å with an angle of 63.0°.

Upon full hydrogenation, not only the structure but also the work functions, cohesive energies and the H binding energies significantly differ from those of the half-hydrogenated structure. The work function of the full-H-PbI_2 is found to be 3.73 eV. The cohesive energy of the full-H-PbI_2 is calculated to be 2.03 eV smaller than that of half-H-PbI_2. The calculated average binding energy of an H atom is 0.93 eV which is larger when compared to those of the single H and half-hydrogenated cases. Here, it is noteworthy that the larger binding energy is consistent with the slightly larger work function. As shown in Fig. 4(d) the full-H-PbI_2 is a semiconductor with an indirect bandgap of 0.76 eV.

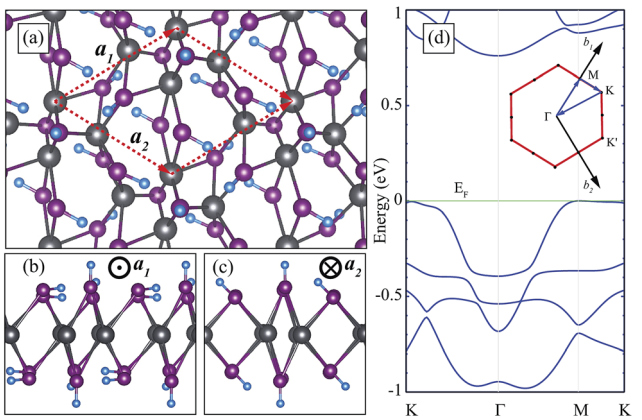

Fig. 4 (a), (b), and (c) illustrate the structure of full-hydrogenated monolayer PbI_2 from the top and side views with the corresponding directions, respectively. (d) is the band structure of full-hydrogenated monolayer PbI_2. The Fermi level (E_F) is given by the green solid line.

The VBM and CBM stay at the M and Γ points which are similar to those of half-H-PbI_2. It is also seen that the Jahn–Teller type distortion in the structure removes dangling bonds and therefore the system is converged to a non-magnetic semiconducting ground state.

VII. Conclusion

In this paper, we studied the newly emerging ultra-thin PbI_2 which is a member of the metal halides. Starting from the comparison of two possible monolayer phases, 1T and 1H, interaction with single H atoms, and half- and full-hydrogenation of monolayer PbI_2 were investigated by performing first principles DFT calculations. The 1T phase was found to be favourable with a bandgap of 2.69 and 1.93 eV within GGA and GGA + SOC, respectively. Our calculations also showed that the H atoms strongly react with the PbI_2 surfaces and further functionalization of its surfaces can be realized. The binding energy was found to be 0.3 eV.

In the case of half-hydrogenation, it was found that the (2 × 1) Jahn–Teller type distorted ground state structure corresponds to the ground state phase. We showed that reconstruction from the perfectly hexagonal structure to 2 × 1 half-H-PbI_2 leads to dramatic modifications such as (i) a metal-to-semiconductor transition and (ii) the removal of magnetic moments. Moreover, our calculations revealed that full-hydrogenated monolayer PbI_2 forms another (2 × 2) Jahn–Teller distorted form in its ground state. In this case, the structure of full-H-PbI_2 was a nonmagnetic semiconductor with a bandgap of 0.76 eV. Our results reveal that hydrogenation is an efficient way to engineer the structural and electronic properties of single layer PbI_2.

Acknowledgements

This work was supported by the bilateral project between TUBITAK (through Grant No. 113T050) and the Flemish Science Foundation (FWO-Vl). The calculations were performed at the TUBITAK ULAKBIM High Performance and Grid Computing Center (TR-Grid e-Infrastructure). CB and HS acknowledge support from TUBITAK Project No. 114F397. H. S. acknowledges support from Bilim Akademisi – The Science Academy, Turkey under the BAGEP program.

References

1 K. S. Novoselov, A. K. Geim, S. V. Morozov, D. Jiang, Y. Zhang, S. V. Dubonos, I. V. Grigorieva and A. A. Firsov, *Science*, 2004, **306**, 666–669.

2 S. Cahangirov, M. Topsakal, E. Akturk, H. Sahin and S. Ciraci, *Phys. Rev. Lett.*, 2009, **102**, 236804.
3 A. Kara, H. Enriquez, A. P. Seitsonen, L. C. L. Y. Voon, S. Vizzini, B. Aufray and H. Oughaddou, *Surf. Sci. Rep.*, 2012, **67**, 1–18.
4 M. E. Davila, L. Xian, S. Cahangirov, A. Rubio and G. Le Lay, *New J. Phys.*, 2014, **16**, 095002.
5 K. Yang, S. Cahangirov, A. Cantarero, A. Rubio and R. D'Agosta, *Phys. Rev. B: Condens. Matter Mater. Phys.*, 2014, **89**, 125403.
6 G. G. Guzman-Verri and L. C. Lew Yan Voon, *Phys. Rev. B: Condens. Matter Mater. Phys.*, 2007, **76**, 075131.
7 F. Bechstedt, L. Matthes, P. Gori and O. Pulci, *Appl. Phys. Lett.*, 2012, **100**, 261906.
8 R. A. Gordon, D. Yang, E. D. Crozier, D. T. Jiang and R. F. Frindt, *Phys. Rev. B: Condens. Matter Mater. Phys.*, 2002, **65**, 125407.
9 J. N. Coleman, M. Lotya, A. O'Neill, S. D. Bergin, P. J. King, U. Khan, K. Young, A. Gaucher, S. De, R. J. Smith, I. V. Shvets, S. K. Arora, J. J. Boland, J. J. Wang, J. F. Donegan, J. C. Grunlan, G. Moriarty, A. Shmeliov, R. J. Nicholls, J. M. Perkins, E. M. Grieveson, K. Theuwissen, D. W. McComb, P. D. Nellist and V. Nicolosi, *Science*, 2011, **331**, 568–571.
10 C. Ataca, H. Sahin and S. Ciraci, *J. Phys. Chem. C*, 2012, **116**(16), 8983–8999.
11 J. S. Ross, P. Klement, A. M. Jones, N. J. Ghimire, J. Yan, D. G. Mandrus, T. Taniguchi, K. Watanabe, K. Kitamura, W. Yao, D. H. Cobden and X. Xu, *Nat. Nanotechnol.*, 2014, **9**, 268–272.
12 H. Sahin, S. Tongay, S. Horzum, W. Fan, J. Zhou, J. Li, J. Wu and F. M. Peeters, *Phys. Rev. B: Condens. Matter Mater. Phys.*, 2013, **87**, 165409.
13 S. Tongay, H. Sahin, C. Ko, A. Luce, W. Fan, K. Liu, J. Zhou, Y.-S. Huang, C.-H. Ho, J. Yan, D. F. Ogletree, S. Aloni, J. Ji, S. Li, J. Li, F. M. Peeters and J. Wu, *Nat. Commun.*, 2014, **5**, 3252.
14 S. Horzum, D. Cakir, J. Suh, S. Tongay, Y.-S. Huang, C.-H. Ho, J. Wu, H. Sahin and F. M. Peeters, *Phys. Rev. B: Condens. Matter Mater. Phys.*, 2014, **89**, 155433.
15 B. Chen, H. Sahin, A. Suslu, L. Ding, M. I. Bertoni, F. M. Peeters and S. Tongay, *ACS Nano*, 2015, **9**, 5326–5332.
16 H. Sahin, S. Changirov, M. Topsakal, E. Bekaroglu, E. Akturk, R. T. Senger and S. Ciraci, *Phys. Rev. B: Condens. Matter Mater. Phys.*, 2009, **80**, 155453.
17 K. K. Kim, A. Hsu, X. Jia, S. M. Kim, Y. Shi, M. Hofmann, D. Nezich, J. F. Rodriguez-Nieva, M. Dresselhaus, T. Palacios and J. Kong, *Nano Lett.*, 2012, **12**, 161–166.
18 P. Tsipas, S. Kassavetis, D. Tsoutsou, E. Xenogiannopoulou, E. Golias, S. A. Giamini, C. Grazianetti, D. Chiappe, A. Molle, M. Fanciulli and A. Dimoulas, *Appl. Phys. Lett.*, 2013, **103**, 251605.
19 C. Bacaksiz, H. Sahin, H. D. Ozaydin, S. Horzum, R. T. Senger and F. M. Peeters, *Phys. Rev. B: Condens. Matter Mater. Phys.*, 2015, **91**, 085430.
20 Y. Aierken, H. Sahin, F. Iyikanat, S. Horzum, A. Suslu, B. Chen, R. T. Senger, S. Tongay and F. M. Peeters, *Phys. Rev. B: Condens. Matter Mater. Phys.*, 2015, **91**, 245413.
21 A. Suslu, K. Wu, H. Sahin, B. Chen, S. Yang, H. Cai, T. Aoki, S. Horzum, J. Kang, F. M. Peeters and S. Tongay, *Sci. Rep.*, 2016, **6**, 20525.
22 D. C. Elias, R. R. Nair, T. M. G. Mohiuddin, S. V. Morozov, P. Blake, M. P. Halsall, A. C. Ferrari, D. W. Boukhvalov, M. I. Katsnelson, A. K. Geim and K. S. Novoselov, *Science*, 2009, **323**, 610–613.
23 M. Z. S. Flores, P. A. S. Autreto, S. B. Legoas and D. S. Galvao, *Nanotechnology*, 2009, **20**, 465704.
24 H. Sahin, C. Ataca and S. Ciraci, *Phys. Rev. B: Condens. Matter Mater. Phys.*, 2010, **81**, 205417.
25 H. Sahin and C. Ciraci, *Phys. Rev. B: Condens. Matter Mater. Phys.*, 2011, **84**, 035452.
26 J. O. Sofo, A. S. Chaudhari and G. D. Barber, *Phys. Rev. B: Condens. Matter Mater. Phys.*, 2007, **75**, 153401.
27 H. Sahin, C. Ataca and S. Ciraci, *Appl. Phys. Lett.*, 2009, **95**, 222510.
28 J. Zhou, M. M. Wu, X. Zhou and Q. Sun, *Appl. Phys. Lett.*, 2009, **95**, 103108.
29 X.-Q. Wang, H.-D. Li and J.-T. Wang, *Phys. Chem. Chem. Phys.*, 2012, **14**, 3031–3036.
30 L. C. Lew Yan Voon, E. Sandberg, R. S. Aga and A. A. Farajian, *Appl. Phys. Lett.*, 2010, **97**, 163114.
31 M. Houssa, E. Scalise, K. Sankaran, G. Pourtois, V. V. Afanasev and A. Stesmans, *Appl. Phys. Lett.*, 2011, **98**, 223107.
32 I. Cabria, M. J. Lopez and J. A. Alonso, *Nanotechnology*, 2006, **17**, 778.
33 H. Shi, H. Pan, Y.-W. Zhang and B. I. Yakobson, *Phys. Rev. B: Condens. Matter Mater. Phys.*, 2013, **88**, 205305.
34 H. Pan, *J. Phys. Chem. C*, 2014, **118**, 13248–13253.
35 M. M. Lee, J. Teuscher, T. Miyasaka, T. N. Murakami and H. J. Snaith, *Science*, 2012, **338**, 643–647.
36 J. Y. Jeng, Y. F. Chiang, M. H. Lee, S. R. Peng, T. F. Guo, P. Chen and T. C. Wen, *Adv. Mater.*, 2013, **25**, 3727–3732.
37 Z. K. Tan, R. S. Moghaddam, M. L. Lai, P. Docampo, R. Higler, F. Deschler, M. Price, A. Sadhanala, L. M. Pazos, D. Credgington, F. Hanusch, T. Bein, H. J. Snaith and R. H. Friend, *Nat. Nanotechnol.*, 2014, **9**, 687–692.
38 M. A. Green, A. Ho-Baillie and H. J. Snaith, *Nat. Photonics*, 2014, **8**, 506–514.
39 Y. Guo, K. Shoyama, W. Sato, Y. Matsuo, K. Inoue, K. Harano, C. Liu, H. Tanaka and E. Nakamura, *J. Am. Chem. Soc.*, 2015, **137**, 15907–15914.
40 A. S. Toulouse, B. P. Isaacoff, G. Shi, M. Matuchova, E. Kioupakis and R. Merlin, *Phys. Rev. B: Condens. Matter Mater. Phys.*, 2015, **91**, 165308.
41 L. Cabana, E. Batista, B. Ballesteros, C. Magn, R. Arenal, J. Or-Sol, R. Rurali and G. Tobias, *Adv. Mater.*, 2014, **26**, 2016–2021.
42 M. Zhou, W. Duan, Y. Chen and A. Du, *Nanoscale*, 2015, **7**, 15168–15174.
43 G. Kresse and J. Hafner, *Phys. Rev. B: Condens. Matter Mater. Phys.*, 1993, **47**, 558.
44 G. Kresse and J. Furthmller, *Phys. Rev. B: Condens. Matter Mater. Phys.*, 1996, **54**, 11169.

45 G. Kresse and D. Joubert, *Phys. Rev. B: Condens. Matter Mater. Phys.*, 1999, **59**, 1758.
46 J. P. Perdew, K. Burke and M. Ernzerhof, *Phys. Rev. Lett.*, 1996, **77**, 3865.
47 S. J. Grimme, *Comput. Chem.*, 2006, **27**, 1787–1799.
48 T. Bucko, J. Hafner, S. Lebegue and J. G. Angyan, *J. Phys. Chem. A*, 2010, **114**, 11814–11824.
49 G. Henkelman, A. Arnaldsson and H. Jonsson, *Comput. Mater. Sci.*, 2006, **36**, 354–360.
50 R. F. W. Bader, *Atoms in Molecules A Quantum Theory*, Oxford University Press, Oxford, UK, 1990.
51 H. Sahin and S. Ciraci, *J. Phys. Chem. C*, 2012, **116**, 24075–24083.